

Effect of time of hydrothermal heat treatment on mesoporous nano-TiO₂ synthesis

L. M. Santos^{1*}, D. J. R. da Silva², M. R. C. Santos³, A. E. H. Machado^{3,4}

¹Instituto Federal de Educação, Ciência e Tecnologia de Goiás, R. Formosa, Qd. 28-29, 76400-000, Uruaçu, GO, Brazil

²Universidade Federal de Pernambuco, Centro de Ciências Exatas e da Natureza, Departamento de Química Fundamental, 50740-560, Recife, PE, Brazil

³Universidade Federal de Catalão, 75704-020, Catalão, GO, Brazil

⁴Universidade Federal de Uberlândia, Instituto de Química, Laboratório de Fotoquímica e Ciência de Materiais, 38400-902, Uberlândia, MG, Brazil

Abstract

Mesoporous TiO₂ nanoparticles were synthesized by the sol-gel method and using hydrothermal treatment at 200 °C during different time intervals, which allowed the evaluation of the time or the treatment on the structural, morphological, and optical properties of the oxides. TEM micrographs showed that the morphology of the materials was characterized by the presence of spherical clusters, while the crystalline phases of the anatase and brookite mixtures were analyzed by X-ray diffraction and Raman spectroscopy. A type IV profile was identified from the results of specific surface area, which is characteristic of the mesoporous material with strong and weak affinity. The band gap in the range of 3.29 and 3.40 eV, estimated by the Kubelka-Munk function, showed a gradual increase as a result of oxide crystallization. It was found that 8 h of treatment in a hydrothermal system was sufficient to synthesize a photocatalyst with optimal photocatalytic performance. This efficiency was probably based on a good correlation between physical and chemical factors, such as high surface area and porosity, the improved capability of photon adsorption in the visible range, crystallinity, and a favorable content of brookite.

Keywords: titanium dioxide, sol-gel synthesis, mesopores, hydrothermal treatment, heterogeneous photocatalysis.


INTRODUCTION

Research involving materials on a nanometric scale has progressed rapidly, owing to their numerous potential applications, in virtue of their optical, electrical, and photoelectrical properties, distinct from materials of conventional size [1]. One of the most promising materials, the nanostructured mesoporous titanium dioxide (TiO₂) has been attracting much attention due to its physical and chemical properties, in addition to the possibility of applications in a wide range of fields, such as catalysis [2], environmental photocatalysis [3, 4], photoluminescence [5], photocatalytic production of hydrogen [6, 7], dye-sensitized solar cells [8, 9], chemical sensors for gases [10], coating in biomedical applications [11], among others. As a ceramic material characterized by its electronic properties, TiO₂ is an n-type semiconductor with the band gap energy of the bulk material extended to the ultraviolet spectrum at approximately 3.20, 3.02, and 3.14 eV, as exhibited by their three natural polymorphs anatase, rutile, and brookite, respectively [12]. The physical and chemical properties of TiO₂ depend on its size, shape, surface area, crystalline phase, and crystallinity degree of the particles. The materials based on TiO₂ are the most used photocatalysts since the discovery of their

photocatalytic properties by Fujishima and Honda [13].

The low crystallinity of TiO₂, whether in the crystalline or amorphous state, tends to be deleterious for photocatalytic applications. In order to achieve a good balance between crystallinity and porosity in the synthesis of mesoporous materials, thermal treatment at mild conditions is necessary [3, 14]. The use of sol-gel conventional methods for the preparation of TiO₂ spherical and monodisperse particles is not efficient due to the fast hydrolysis rate of the precursors, which interferes with the nucleation and growth of the nanoparticles. In this regard, in a modified sol-gel synthesis route, reagents, such as glycols, that act as structural mold are used. These reagents favor the controlled formation of critical cores, leading ultimately to mesoporous nanometric particles. The hydrothermal processing approach has many advantages when compared to other conventional approaches, such as low cost, low temperature of treatment, and control of size and morphology of the final product. The advantages of controlled experimental conditions in the thermal treatment in the formation of crystalline catalysts include the narrow distribution of the particle size and high levels of purity, surface area, and porosity [15]. However, TiO₂ as a photocatalyst exhibits some disadvantages that still need to be overcome for the sake of commercial applications. High band gap energies and a high rate of recombination of charge carriers (electron/hole, e⁻/h⁺, pair) are the main issues to be solved since they reduce considerably the quantum yield of the photocatalytic process [16-18].

*lidiaine.santos@ifg.edu.br

 <https://orcid.org/0000-0002-5570-9899>

Lin *et al.* [19] demonstrated that the brookite phase is a photocatalyst of great potential owing to its band gap energy close to that of the anatase phase. Therefore, a blend of anatase/brookite phases should present the potential to become a better photocatalyst as compared to pure anatase, due to the better separation of the charge carriers in the blend. With these considerations in mind, the influence of the thermal treatment duration via the hydrothermal (HT) processing was studied, upon the structural, morphological, and electronic properties of mesoporous TiO_2 prepared by the modified sol-gel method using ethylene glycol as a structural mold. The photocatalytic activity was assessed by monitoring the degradation of the azo dye Ponceau 4R (P4R), chosen due to its toxicity [20].

MATERIALS AND METHODS

Synthesis of the oxides: all chemical reagents used in this work were of high purity and used as received. A mixture of 50 mL (886 mmol) of ethylene glycol (Vetec, 99.5%) and 10 mL of titanium isopropoxide (IV) (Aldrich, 97%) was prepared and kept under magnetic stirring at 25 °C for 2 h. Afterward, 10 mL of ultrapure water and 90 mL of acetone (Synth, 99.5%) were added to the suspension, keeping the system under vigorous stirring also at 25 °C for 2 h. The white precipitate was extracted by centrifugation (9000 rpm for 20 min), followed by several washes using ethanol in order to remove any glycol residue. Subsequently, the precipitate was washed with distilled water three times and dried in a muffle at 70 °C for 12 h. The resulting material, TiO_2G , was submitted to a thermal treatment via hydrothermal (HT) route in a Teflon reactional glass kept in a reactor at 200 °C and under the pressure of approximately 12.8 bar. Different durations of the HT process were tested: 2, 4, 6, 8, 10, and 12 h. The TiO_2 samples were labeled according to the time of the HT treatment, as HT2, HT4, HT6, HT8, HT10, and HT12, respectively.

Characterization: the thermal characterization (thermal gravimetry/differential thermal analysis - TG/DTA) of the photocatalysts was carried out using a thermal analyzer (DTG-60H, Shimadzu) with ± 5 °C of accuracy, in a nitrogen atmosphere with a heating rate of 10 °C.min⁻¹ and a temperature scanning from 25 to 1000 °C. The high-resolution transmission electron microscopy (TEM) images were acquired with a microscope (JEM-2100, Jeol). The X-ray diffraction (XRD) analyses were performed in a diffractometer (XRD600, Shimadzu) with operation parameters set at 40 kV and 120 mA, using $\text{CuK}\alpha$ radiation ($\lambda=1.54148$ Å). The diffractograms were treated using the software FullProf. The crystallite sizes were calculated from the data obtained from Rietveld refinement. An ASAP 2010 analyzer (Micrometrics) was used to measure adsorption-desorption isotherms of N_2 , and the data was modeled according to the BET model for specific surface area and the Barrett-Joyner-Halenda (BJH) method for the pore volume determination [21]. The Raman spectra of the samples were acquired at room temperature in a spectrometer (RFS 100/S,

Bruker) equipped with a 1064 nm laser (100 mW) as the excitation source. The measurements of diffuse reflectance were conducted in a spectrometer (UV-1650PC, Shimadzu), and the band gap energy was estimated by the Kubelka-Munk function [22]. Potassium bromide was used as a reference in these experimental measures.

Photocatalytic activity: the activity of the prepared materials was estimated by monitoring the degradation of the Ponceau 4R dye, which is the trisodium (8Z)-7-oxo-8-[(4-sulphonatonaphthalen-1-yl)hydrazinylidene]naphthalene-1,3-disulphonate, Cl 16255 (Sigma-Aldrich, 75%), at the UVA spectral range. The details of the experimental setting were described elsewhere [23]. A 400 W high-pressure mercury lamp, with a photon flux of 3.3×10^6 einstein.s⁻¹, was used as a radiation source (with the UVA irradiance level of 1100 W.m⁻²) [24]. A mixture of 100 mg.L⁻¹ of the catalyst was added to the 31 mg.L⁻¹ of an aqueous solution of the dye (at pH 6.9) prepared under magnetic stirring (with an irradiated volume of 4 L). Next, the mixture was irradiated for 140 min at 40 ± 2 °C and kept under stirring for 30 min in the dark (in order to reach the adsorption equilibrium). Aliquots were collected at intervals of 20 min, then filtered and analyzed in the spectrophotometer (UV-1650PC, Shimadzu) at 507 nm, and using total organic carbon measurements in a TOC-VCPH/CPN analyzer (Shimadzu). The results presented in this work represent the average of three individual experiments. Control assays in the absence of any photocatalyst were also conducted, aiming to identify the role of TiO_2 on the photochemical reaction.

RESULTS AND DISCUSSION

In order to find the optimal thermal treatment conditions, the temperatures of phase transition, and the thermal stability of the synthesized oxides, a TG/DTA thermal analysis was conducted on the produced TiO_2 . The TG and DTA curves are shown in Fig. 1. From the TG curve, it was observed that the mass loss occurred in two expressive steps. The first, at approximately 76.5 °C, was caused by dehydration of the sample, whereas the other, which occurred at approximately 289 °C, should be related to mass loss of the desorption of water molecules physically adsorbed on the material structure as well as chemisorbed species, namely, organic solvent groups such as acetone and glycol fragments employed in the treatment of the sample [25]. Above 300 °C, no significant loss of mass as a function of temperature was observed. The TG analysis versus the data from DTA analysis was interpreted as the mass loss versus the energy change involved in those events (Fig. 1). At 42 °C, an exothermic event was identified, which was related to the elimination of volatile material still present in the crystalline structure. At 228 and 428 °C, the exothermic peaks were attributed to the elimination of structural water and organic matter remnant from the synthesis of the crystalline material [26]. The peak at 373 °C, on the other hand, was endothermic and caused by the ordering processes of crystallinity and crystallization, that is, the conversion of anatase titanium dioxide to rutile

titanium dioxide. The irreversible phase transition from the anatase metastable phase to the thermodynamically stable rutile phase started at around 400 °C and depended on the synthesis route. According to the literature, this is the initial temperature of the crystallization process of the samples obtained from the alkoxide as a precursor, a nonconventional chemical route [26]. Another region showing an endothermic process was observed from 497 to 600 °C, which, according to the literature, was related to the stabilization of the crystalline structure of rutile. This stabilization generally occurs between 500 and 600 °C [27, 28]. A new endothermic band started at around 700 °C and, by analyzing the curve of mass loss, almost no loss was observed, which means that, from 700 °C and beyond, the system absorbed more energy related to the event of another structural transition, perhaps from tetragonal rutile to orthorhombic brookite. At approximately 930 °C, a new, narrow, and low-intensity endothermic peak appeared, which can be attributed to phase transition from brookite to rutile, as predicted by the literature [29]. At 840 and 970 °C, two exothermic peaks were observed, which arose from the elimination of remnant carbonates and hydroxyls trapped in the crystalline structure. This was confirmed by the TG curve, in which a small loss of mass, proportional to the energy intensity, was observed. In general, exothermic peaks in the DTA curve, accompanied by mass loss as shown by TG data, are attributed to matter elimination, whereas endothermic peaks, identified in regions of TG without mass loss, are originated from the structural reorganization processes and phase transitions, like those observed in the current study.

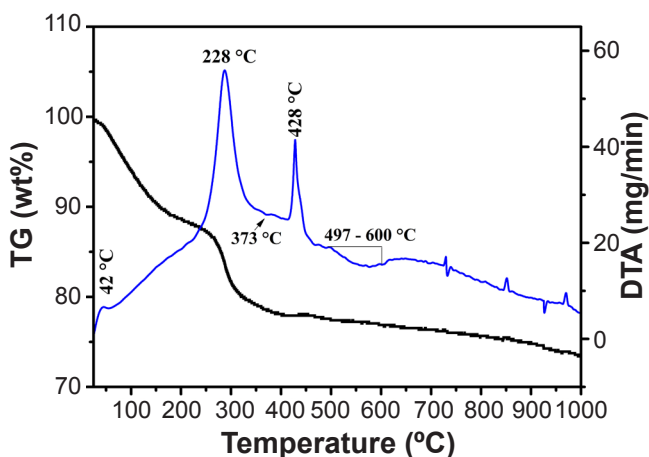


Figure 1: TG and DTA curves of the TiO_2G powder, without heat treatment.

Given the knowledge of the behavior of the samples towards the temperature changes, the temperature for the thermal treatment, after the use of the hydrothermal system, was defined to obtain the desired crystallographic phase for the powders under study. The chosen temperature was 200 °C, followed by a study of the exposure time, seeking the best response from the catalytic profile. After the proper thermal treatments by the hydrothermal (HT) protocol

were performed, the samples were characterized by X-ray diffraction (XRD), transmission electron microscopy (TEM) followed by the photocatalysis characterization methods. The morphology and the (micro)structure of the photocatalysts (samples of HT thermal treatment of 4 and 8 h, respectively, HT4 and HT8) were determined by TEM, XRD, and adsorption/desorption isotherms of $\text{N}_2(\text{g})$. It was observed, from TEM micrographs, that the oxides presented a morphology characterized by the presence of clusters of particles apparently spherical in shape (Figs. 2a and 2b). The estimated average sizes from the high-resolution images (Figs. 2c and 2d) were 2.0 and 4.7 nm for the photocatalysts HT4 and HT8, respectively. Reyes-Coronado *et al.* [30] suggested that, for the case of the anatase, the particle radius varies from 3 to 6 nm for an HT processing conducted at 200 °C, so that an increase in temperature and time of treatment increases the mass transport rate that occurs from particle to particle. Such a process is responsible for particle growth/widening. Additionally, from TEM analysis it was possible to find the crystallographic plane through which the particle growth preferentially took place. From the theory of diffraction:

$$n\lambda = 2d \cdot \sin\theta \quad (\text{A})$$

where λ is the radiation wavelength of XRD, d is the interplanar distance, n is the order of the reflection, and θ is the diffraction angle. Thus, by using Eq. A and the separation between the interatomic planes observed in the TEM micrographs, it was possible to estimate an interplanar distance of 0.35 nm, which corresponded to the crystallographic planes (101) of anatase [31]. The presence of crystallographic planes of rutile was not observed. In the case of the brookite phase, the spacing between the crystallographic planes was of the order of 0.38 nm, which belongs to the planes (120) and (111). This value was very close to the spacing of the anatase (0.35 nm) [32], which hampered the analysis. Despite this, the value related to anatase was confirmed in all samples. Hence, this result was evidence of the predominance of the crystallographic planes of anatase over the possible presence of brookite.

From the analysis of the XRD patterns as a function of HT thermal treatment duration (Fig. 3), the diffraction peaks of the anatase phase of TiO_2 (JCPDS 21-1272) were observed, along with the presence of traces of brookite phase (JCPDS 29-1360). The presence of brookite in all the HT-treated samples may be related to structural distortions caused by the mentioned treatment [33]. In the case of the sample TiO_2G (without thermal treatment) no well-defined peaks could be observed in the XRD pattern, suggesting the sample was amorphous and showing that there was no formation of anatase or brookite before thermal treatment (Fig. 4). Li *et al.* [34] found that the selective formation of different phases of TiO_2 polymorphs strongly depends on the physical-chemical characteristics of the system, such as type of precursors, selective phase additives, temperature, and time of the hydrothermal treatment. For instance, Cihlar *et al.*

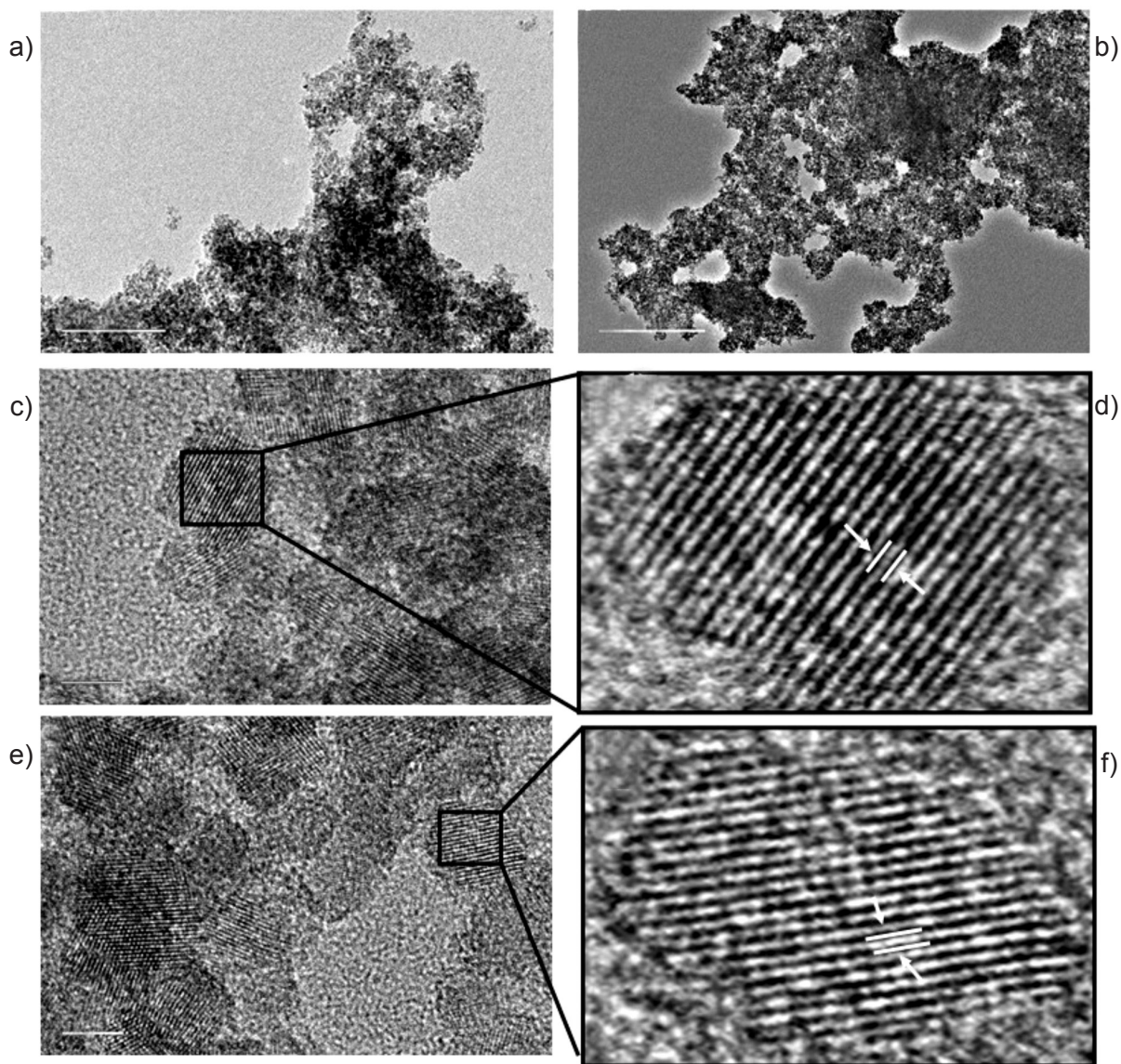


Figure 2: TEM (a,b) and high resolution TEM (c-f) images of HT4 (a,c,d) and HT8 (b,e,f) TiO_2 samples synthesized by the modified sol-gel method; in (d,f), regions selected to measure the interplanar distances.

[35] observed the formation of anatase and brookite in TiO_2 nanoparticles when they were prepared by hydrolysis and (poly)condensation of soluble complexes of titanium under mild hydrothermal conditions, thereby obtaining efficient compounds for photocatalytic production of hydrogen.

The Rietveld refinement of the XRD data shown in Fig. 5, with the main parameters presented in Table I, confirmed the direct relationship between the extension of thermal treatment and the average crystallite size, as verified in Table II. This trend was expected in virtue of the aggregation-recrystallization processes, which, in turn, are influenced by the synthesis procedure. It was observed that the increase of HT treatment duration induced the decrease of the amount of brookite fraction and increased the crystallinity of the material. This was a consequence of the fact that the increase of the time of HT treatment increased the solubility of the crystallites, which ultimately led to an

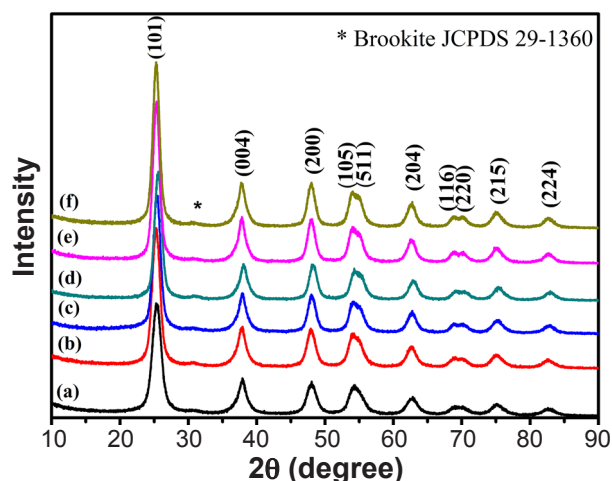


Figure 3: X-ray diffractograms of the TiO_2 catalysts: a) HT2; b) HT4; c) HT6; d) HT8; e) HT10; and f) HT12.

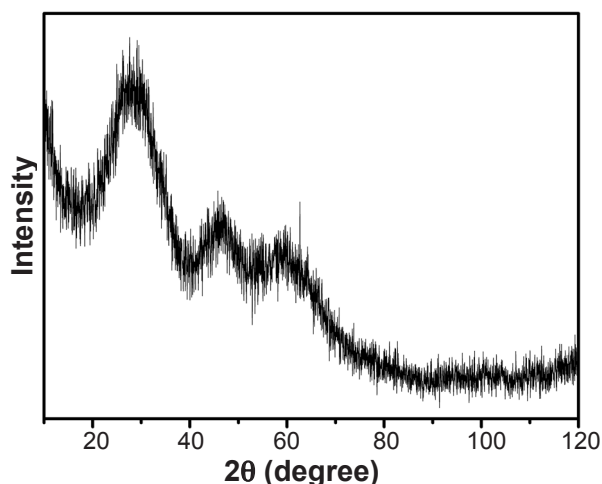


Figure 4: X-ray diffractogram of the TiO₂G (without thermal treatment).

increase of crystallinity and a reduction in the secondary phase (brookite) content.

The adsorption/desorption isotherms of the samples (Fig. 6) showed a profile of type IV, with H3 hysteresis curves, characteristic of mesoporous materials with both strong and weak affinity. Specific surface area and porosity data are presented in Table II. The high surface area observed in the oxides was not affected by the aggregation of the particles. The samples submitted to HT treatment for longer periods (10 and 12 h) showed lower surface area, as a result of better sintering of the particles, and larger crystallite sizes. The sample HT2 presented the lowest porosity as compared to the others, probably due to the short time of HT processing, which was found to be insufficient for the formation of pores. On the other hand, this sample exhibited the highest specific surface area of all the samples studied. This result can be attributed to the presence of materials not yet converted into TiO₂. In addition, from the isotherm analysis, it was observed that the use of ethylene glycol resulted in materials with higher specific surface areas than the other materials based on TiO₂ synthesized by the sol-gel method without ethylene glycol as structural mold [36]. Most probably, this was a consequence of the similarity between the molecular structures of ethylene glycol and titanium isopropoxide (IV), which favored the dispersion of the titanium centers during hydrolysis. Ultimately, this explains the long-term precipitation process, which favored the adhesion of the dispersed centers that converged to form TiO₂ particles with lower surface area.

The catalysts were also studied by Raman spectroscopy (Fig. 7), which evidenced that all samples exhibited vibrational modes typical of the anatase crystalline phase ($A_{1g} + 2B_{1g} + 3E_g$), with the A_{1g} mode overlapped with the peak at 537 cm⁻¹ of the B_{1g} mode [37, 38]. From these results, taking the E_g vibrational mode at 150 cm⁻¹ as a reference, one realizes that the vibrational modes tended to undergo a band widening as the time of hydrothermal processing decreased. This behavior could be explained by the finite lifetime of the vibrational modes exhibited by the smaller particles,

along with their low crystallinity [37]. Such behavior was expected since the samples thermally treated for a shorter hydrothermal period favored the disorder in the structure of TiO₂, which limited the particle growth. These results were in agreement with those of the XRD and high-resolution TEM. Besides the anatase, the presence of brookite was confirmed in all samples, as evidenced by the presence of its vibrational mode peaks at 230 and 350 cm⁻¹ (inset in Fig. 7). Also, the Rietveld refined data (Table I) showed that the content of brookite diminished with the increase of HT treatment duration, which justified the narrowing of the full width at half maximum (FWHM) observed in the band of E_g vibrational mode.

The absorption spectra, expressed in terms of Kubelka-Munk's function $[F(R)]$ versus photon energy (E), related to the studied oxides, derived from diffuse reflectance spectra (Fig. 8 - inset), are presented in Fig. 8. TiO₂ is an indirect semiconductor [39], which implies that the indirect value of the band gap can be estimated by the extrapolation of the linear segment to the intercept with the abscissa of the plot (Table II). The values of E , obtained by the indirect method suggested that the synthesized TiO₂ particles exhibited a quantum confinement effect due to their size since the calculated values of band gap of these samples were greater than those of the bulk TiO₂ (3.20 eV) [16, 40]. The increased band gap exhibited by the samples calcined at high temperatures was related to a more efficient crystallization of the oxides (Table II). On the other hand, it was known that the presence of brookite tended to slow down the recombination of charge carriers due to the energy barrier between the conduction bands of anatase and brookite, which resulted in the entrapment of electrons in the anatase and holes in the brookite phase [6], ultimately facilitating the photocatalytic activity.

The photocatalytic activity of the samples was assessed against the degradation of Ponceau 4R. The control experiment, conducted in the absence of any photocatalyst, revealed very low levels of decolorization (4.0%) and mineralization (13%) of the dye after 140 min of irradiation (Fig. 9). The mineralization efficiency was found to be a function of the time of hydrothermal treatment, reaching a maximum after 8 h for the oxide HT8. For this sample, mineralization of 73% was achieved, with an observed mineralization constant (k_{obs}) of $(9.2 \pm 0.3) \times 10^{-3} \text{ min}^{-1}$ ($R=0.9885$), followed by a decline for longer periods. This result remarks the importance of controlling the time of HT processing, which showed to be decisive for obtaining oxides with optimized photocatalytic activity. The mineralization efficiencies for the different photocatalysts are summarized in Table III. For all the photocatalysts, the mineralization followed a pseudo-first-order rate law with respect to the concentration of the azo dye (Fig. 10a). This process occurs in a step of kinetic constants apparently determined by the availability of reactive oxygen species (ROS), such as hydroxyl (HO•) and superoxide (O₂•-) radicals [18]. It was observed that all samples showed a similar degradation profile, with a reduction of the absorption bands under the

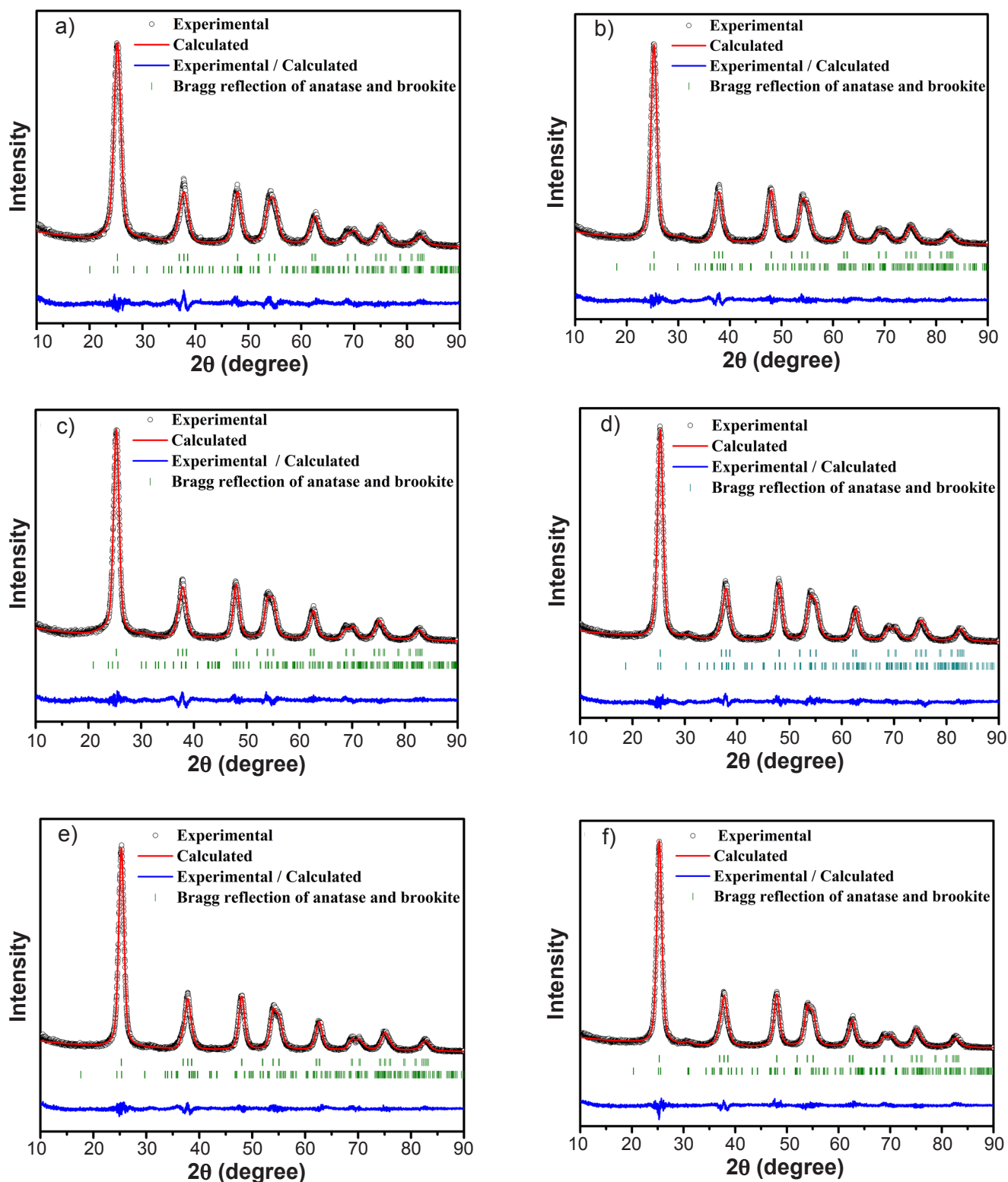


Figure 5: XRD patterns after structural refinement procedure using the Rietveld method: a) HT2; b) HT4; c) HT6; d) HT8; e) HT10; and f) HT12.

action of all the oxides studied, without the appearance of any new absorption band within the spectral region studied. Based on these results, it is suggested that the degradation process must consist of a significant fragmentation of the molecular structure of the dye, which results in its gradual mineralization, although it does not result in the formation

of any noticeable chromophore.

From the photocatalysis results, the observed decolorization for all the samples was 100%, which should be directly related to the homolytic cleavage of the azo bond. The hydroxyl radicals formed at the TiO_2 /solution interface must be one of the main agents responsible for this

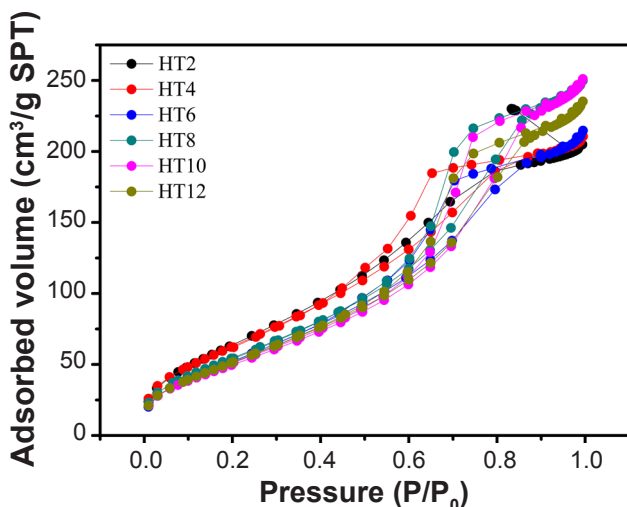
Table I - Quality scores for the Rietveld refinement of the synthesized photocatalysts.

Catalyst	χ^2	S ^a	R _{wp} ^b (%)	R _{Bragg} ^c (%)	Composition phase* (%)	Crystallinity (%)
HT2	2.08	1.44	8.85	6.13	82 (A)+18 (B)	64
HT4	1.99	1.41	8.47	6.01	81 (A)+19 (B)	65
HT6	1.78	1.33	8.13	6.10	82 (A)+18 (B)	66
HT8	2.21	1.47	9.13	6.14	91 (A)+9 (B)	69
HT10	2.00	1.41	8.59	6.08	93 (A)+7 (B)	68
HT12	1.92	1.27	7.69	6.04	95 (A)+5 (B)	71

^a: goodness-of-fit ($S=R_{wp}/R_{Exp}$), ^b: adequation of the observed and calculated profiles; ^c: weighted profile factor; *: A: anatase, B: brookite.

Table II - Structural and electronic properties of the synthesized photocatalysts.

Catalyst	Crystallite size (nm)	Surface area (m ² .g ⁻¹)	Porosity (%)	Band gap (eV)
HT2	5.2	247±4	16	3.29±0.02
HT4	5.9	240±5	31	3.30±0.02
HT6	6.4	203±5	31	3.27±0.01
HT8	6.4	211±3	35	3.28±0.02
HT10	6.7	191±3	35	3.38±0.03
HT12	6.8	198±4	33	3.40±0.02

Figure 6: N₂(g)-adsorption/desorption isotherms for the TiO₂ catalysts.

process [20]. Fig. 10b presents the decolorization profiles related to the action of the photocatalyst HT8. Although these percentages of mineralization depend on the method of synthesis [35], the results suggested that the photocatalytic activity of TiO₂ can be enhanced considering the optimal amount of brookite between 20 and 40 wt% [41], in a binary system composed of anatase and brookite. Shen et al. [42] synthesized nanoparticles of TiO₂ by heating, at 200 °C, a suspension obtained from the addition of tartaric acid and NaOH to an aqueous solution of TiCl₃. In their work, the control of anatase and brookite content was achieved by varying the molar ratio between the tartaric acid and titanium. The sample containing the lowest amount of brookite (21.3% of brookite and 78.7% of anatase) presented

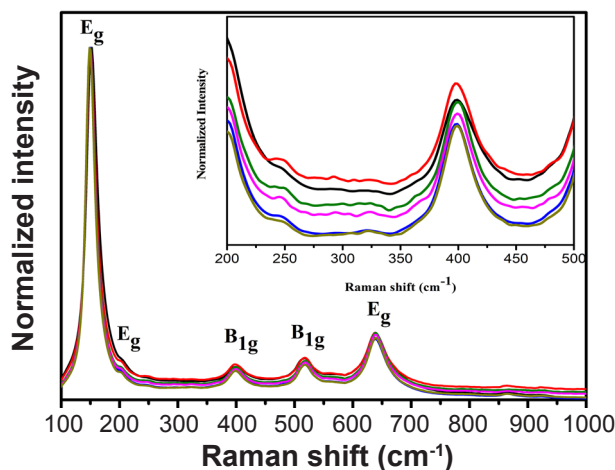


Figure 7: Raman spectra obtained for the different synthesized catalysts: (-) HT2, (-) HT4, (-) HT6, (-) HT8, (-) HT10, (-) HT12. Inset: normalized spectra showing the region of the vibrational modes of the brookite phase.

the highest photocatalytic activity in the degradation of the Rhodamine B dye when compared to the catalysts made of either brookite or anatase in their pure states. The photocatalytic activity of a semiconductor depends on many factors. The best photocatalytic performance of HT8, when compared with the remaining synthesized oxides, can be explained by a combination of physical and chemical factors. This catalyst formulation displayed a high surface area and porosity, crystallinity, and high absorption capacity of photons of the UV-visible region of the spectrum, as well as a good content of brookite. Such factors combined were able to improve the efficiency in the production of the reactive

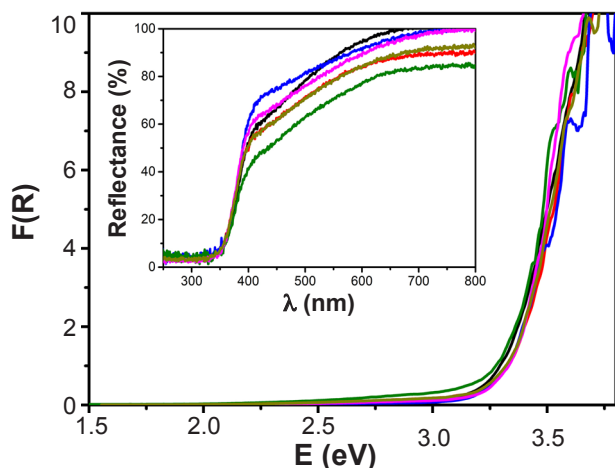


Figure 8: Relation between $F(R)$ and the incident photon energy (E) for the synthesized catalysts: (—) HT2, (—) HT4, (—) HT6, (—) HT8, (—) HT10, (—) HT12. Inset: diffuse reflectance spectra of the catalysts.

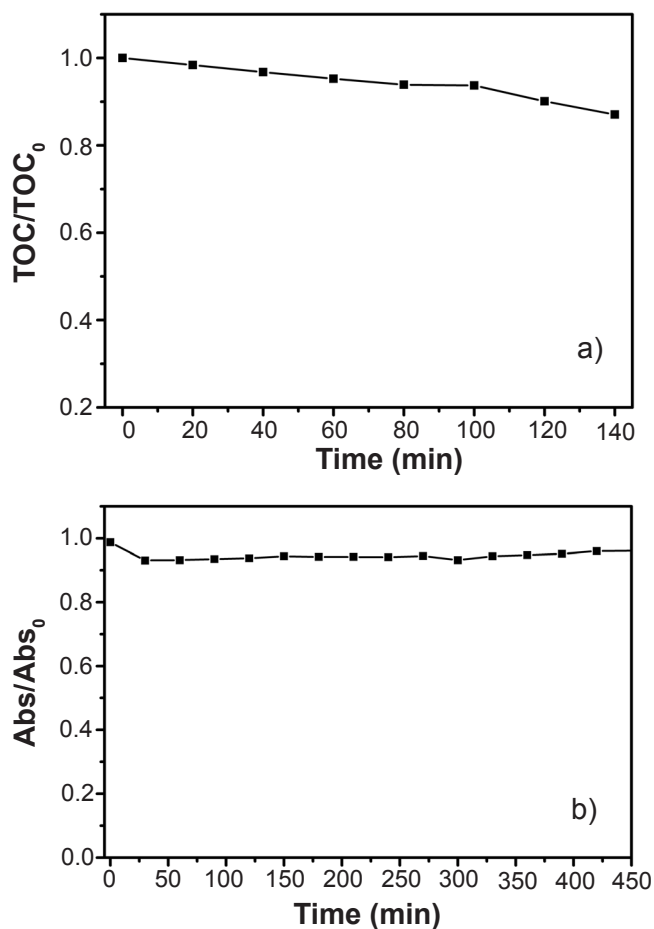


Figure 9: Variation of the normalized total organic carbon, TOC/TOC_0 (a), and decolorization, Abs/Abs_0 (b), as a function of the photolysis time of a pH 6.9 Ponceau 4R dye aqueous solution in the absence of any catalyst.

oxygen species (ROS) responsible for the degradation and mineralization of the organic substrate. Additionally, the minimization of e^-/h^+ pairs recombination should not be neglected, since it allows the availability of the holes for the

Table III - Photocatalytic performance of the prepared oxides in terms of P4R dye degradation.

Photocatalyst	Mineralization (%)	k_{obs} (10^{-3} min^{-1})
HT2	41	3.5 ± 0.2
HT4	58	5.8 ± 0.3
HT6	55	5.8 ± 0.2
HT8	73	9.2 ± 0.3
HT10	66	7.4 ± 0.2
HT12	65	7.3 ± 0.3

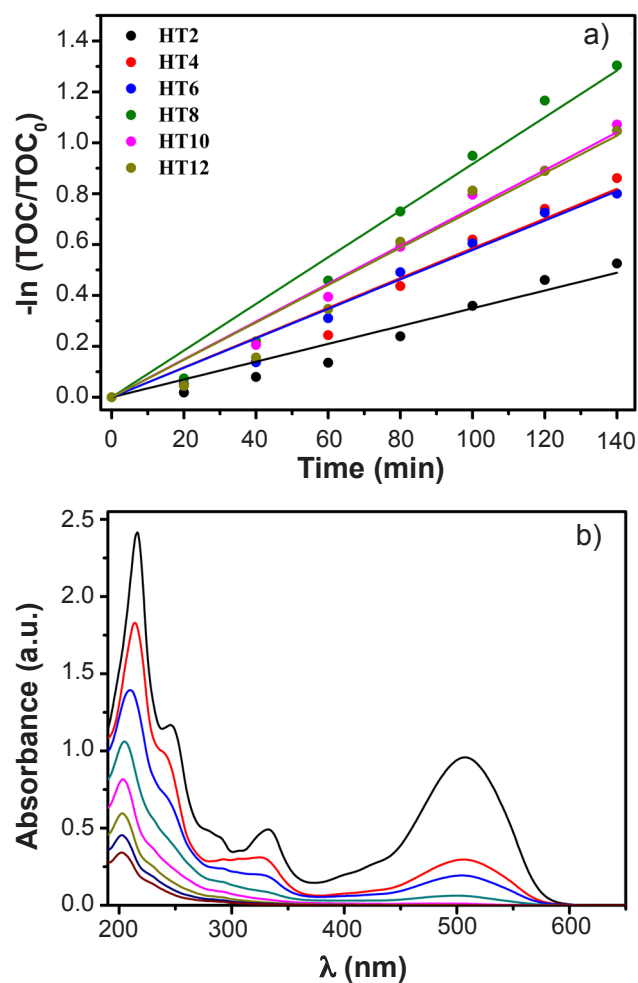


Figure 10: Results of P4R mineralization kinetics in the presence of different TiO_2 photocatalysts (a) and UV-vis spectra of the dye solution as a function of the irradiation time ($\Delta t=20$ min) using HT8 photocatalyst (b).

oxidation reactions. The outcome of these combined effects was the drastic improvement of the photocatalytic activity of the synthesized material.

CONCLUSIONS

Mesoporous nanoparticles of TiO_2 with optimized photocatalytic activity were prepared by the sol-gel method

employing ethylene glycol as a structural mold, followed by the hydrothermal treatment. The synthesized oxides, a mixture of the anatase and brookite phases, exhibited a predominance of the anatase crystalline phase, regardless of the time of thermal treatment. However, the time of hydrothermal treatment influenced the brookite content, so that an increase in the treatment time reduced the amount of brookite, along with an increase in the crystallinity of the oxides. The photocatalytic activity was found to be most significant for the TiO₂ HT8 sample (hydrothermally treated at 200 °C for 8 h), a result that was justified by the formation of binary oxides characterized by the presence of anatase and brookite, high BET surface area, nanoscale size, and mesoporosity. The combination of these factors improved the quantum yield for reactive oxygen species (ROS) formation.

ACKNOWLEDGMENTS

The authors thank the Brazilian research agencies, Fundação de Amparo à Pesquisa do Estado de Minas Gerais - FAPEMIG, and Conselho Nacional de Desenvolvimento Científico e Tecnológico - CNPq, for the research support; to the Centro de Tecnologias Estratégicas do Nordeste - CETENE, and the Laboratório Multiusuário de Microscopia de Alta Resolução - LABMIC, for the support in the powder characterizations; L. M. Santos is particularly grateful to Coordenação de Aperfeiçoamento de Pessoal de Nível Superior - CAPES, for her scholarship.

REFERENCES

- [1] S.V. Nipane, S.W. Lee, G.S. Gokavi, A.N. Kadam, J. Mater. Sci. Mater. Electron. **29**, 19 (2018) 16553.
- [2] S. Riyapan, Y. Zhang, A. Wongkaew, B. Pongthawornsakun, J.R. Monnier, J. Panpranot, Catal. Sci. Technol. **6** (2016) 5608.
- [3] A.E.H. Machado, K.A. Borges, T.A. Silva, L.M. Santos, M.F. Borges, W.A. Machado, B.P. Caixeta, S.M. Oliveira, A.G. Trovó, A.O.T. Patrocínio, in "Solar radiation applications", S.R. Bello (Ed.), IntechOpen (2015) 87.
- [4] K. Santhi, M. Navaneethan, S. Harish, S. Ponnusamy, C. Muthamizhchelvan, Appl. Surf. Sci. **500** (2020) 144058.
- [5] K.K. Paul, S. Jana, P.K. Giri, Part. Part. Syst. Charact. **35**, 9 (2018) 1800198.
- [6] A.O.T. Patrocínio, J. Schneider, M.D. França, L.M. Santos, B.P. Caixeta, A.E.H. Machado, D.W. Bahnemann, RSC Adv. **5** (2015) 70536.
- [7] Z. Tay, Q.L. Liu, X.F. Tang, Y.X. Jiang, Z.L. Sum, T.C. Chen, J. Phys. Chem. C **117** (2013) 14973.
- [8] L.F. Paula, R.C. Amaral, N.Y. Murakami Iha, R.M. Paniago, A.E.H. Machado, A.O.T. Patrocínio, RSC Adv. **4**, 20 (2014) 10310.
- [9] M. Pastore, T. Etienne, F. De Angelis, J. Mater. Chem. C **4** (2016) 4346.
- [10] O. Alev, E. Şennik, N. Kiliç, Z.Z. Öztürk, Procedia Eng. **120** (2015) 1162.
- [11] S. Kaur, N. Bala, C. Khosla, Anti-Corros. Methods Mater. **66**, 1 (2019) 74.
- [12] M. Grätzel, F.P. Rotzinger, Chem. Phys. Lett. **118**, 5 (1985) 474.
- [13] A. Fujishima, K. Honda, Nature **238** (1972) 37.
- [14] R.A. Sacramento, O.M.S. Cysneiros, B.J.B. Silva, A.O.S. Silva, Cerâmica **65**, 376 (2019) 585.
- [15] P. Maheswari, S. Ponnusamy, S. Harish, M.R. Ganesh, Y. Hayakawa, Arab. J. Chem. **13**, 1 (2020) 3484.
- [16] L.G. Kumar, S.G. Devi, J. Phys. Chem. A **115** (2011) 13211.
- [17] H. Feng, M.H. Zhang, L.E. Yu, Appl. Catal. A Gen. **413** (2012) 238.
- [18] M.D. França, L.M. Santos, T.A. Silva, K.A. Borges, V.M. Silva, A.O.T. Patrocínio, A.G. Trovó, A.E.H. Machado, J. Braz. Chem. Soc. **27** (2016) 1094.
- [19] H. Lin, L. Li, M. Zhao, X. Huang, X. Chen, G. Li, R. Yu, J. Am. Chem. Soc. **134**, 20 (2012) 8328.
- [20] S.G.F. Aguilar, U.R. Charrondiere, B. Dusemund, P. Galtier, J. Gilbert, D.M. Gott, I.M.C.M.R. Guertler, J. Koenig, C. Lambré, J.-C. Larsen, J.-C. Leblanc, A. Mortensen, D. Parent-Massin, I. Pratt, R.A.W. Rietjens, I. Stankovic, P. Tobback, T. Verguieva, EFSA J. **7**, 11 (2009) 1.
- [21] E.P. Barrett, L.G. Joyner, P.P. Halenda, J. Am. Chem. Soc. **73**, 1 (1951) 373.
- [22] E.M. Patterson, C.E. Shelden, B.H. Stockton, Appl. Opt. **16** (1977) 2627.
- [23] D.F.M. Oliveira, P.S. Batista, P.S. Muller, V. Velani, M.D. Frana, D.R. De Souza, A.E.H. Machado, Dyes Pigm. **92**, 1 (2012) 563.
- [24] A.E.H. Machado, M.D. França, V. Velani, G.A. Magnino, H.M. Velani, F.S. Freitas, P.S. Müller, C. Sattler, A. Schmucker, Int. J. Photoenergy **2008** (2008) 482373.
- [25] S.D. Delekar, H.M. Yadav, S.N. Achary, S.S. Meena, S.H. Pawar, Appl. Surf. Sci. **263** (2012) 536.
- [26] M.M. Viana, V.F. Soares, N.D.S. Mohallem, Ceram. Int. **36**, 7 (2010) 2047.
- [27] P.S. Ha, H.J. Youn, H.S. Jung, K.S. Hong, Y.H. Park, K.H. Ko, J. Colloid Interf. Sci. **223**, 1 (2000) 16.
- [28] Q.H. Zhang, L. Gao, J.K. Guo, NanoStruct. Mater. **11**, 8 (1999) 1293.
- [29] A. Di Paola, G. Cufalo, M. Addamo, M. Bellardita, R. Campostrini, M. Ischia, R. Ceccato, L. Palmisano, Colloids Surf. A Physicochem. Eng. Asp. **317** (2008) 366.
- [30] D. Reyes-Coronado, G. Rodriguez-Gattorno, M.E. Espinosa-Pesqueira, C. Cab, R. De Coss, G. Oskam, Nanotechnology **19**, 14 (2008) 145605.
- [31] N. Wu, J. Wang, D.N. Tafen, H. Wang, J.G. Zheng, J.P. Lewis, X. Liu, S.S. Leonard, A. Manivannan, J. Am. Chem. Soc. **132**, 19 (2010) 6679.
- [32] M. Kobayashi, V.V. Petrykin, M. Kakihana, K. Tomita, M. Yoshimura, Chem. Mater. **19**, 22 (2007) 5373.
- [33] S. Naghibi, M.A. Faghihi Sani, H.R. Madaah Hosseini, Ceram. Int. **40**, 3 (2014) 4193.
- [34] J.G. Li, T. Ishigaki, X. Sun, J. Phys. Chem. C **111**, 13 (2007) 4969.
- [35] J. Cihlar, V. Kasperek, M. Kralova, K. Castkova, Int. J.

Hydrog. Energy **40**, 7 (2015) 2950.

[36] M.A. Behnajady, H. Eskandarloo, N. Modirshahla, M. Shokri, Desalination **278**, 1 (2011) 10.

[37] X. Chen, Y. Low, A.C.S. Samia, C. Burda, J.L. Gole, Adv. Funct. Mater. **15**, 1 (2005) 41.

[38] H. Fang, C.X. Zhang, L. Liu, Y.M. Zhao, H.J. Xu, Biosens. Bioelectron. **64** (2015) 434.

[39] F.P. Koffyberg, K. Dwight, Solid State Commun. **30**, 7

(1979) 433.

[40] U. Diebold, Surf. Sci. Rep. **48**, 5 (2003) 53.

[41] R. Boppella, P. Basak, S.V. Manorama, ACS Appl. Mater. Interfaces **4**, 3 (2012) 1239.

[42] X. Shen, J. Zhang, B. Tian, M. Anpo, J. Mater. Sci. **47**, 15 (2012) 5743.

(*Rec. 15/09/2020, Rev. 31/01/2021, 05/05/2021, 02/06/2021, Ac. 06/06/2021*)

